Characterization of ascending aortic flow in patients with degenerative aneurysms a 4D flow magnetic resonance study

Ramaekers, M.J.F.G.; Adriaans, B.P.; Juffermans, J.F.; Assen, H.C. van; Bekkers, S.C.A.M.; Scholte, A.J.H.A.; ... ; Schalla, S.

OPEN

Characterization of Ascending Aortic Flow in Patients With Degenerative Aneurysms

A 4D Flow Magnetic Resonance Study

Mitch J.F.G. Ramaekers, MD,†‡§ Bouke P. Adriaans, MD,*†‡ Joe F. Juffermans, MSc,§ Hans C. van Assen, PhD,§ Sebastiaan C.A.M. Bekkers, MD, PhD,*†‡ Arthur J.H.A. Scholte, MD, PhD,|| Sasa Kenjeres, PhD,¶ Hildo J. Lamb, MD, PhD,§ Joachim E. Wildberger, MD, PhD,*‡ Jos J.M. Westenberg, PhD,§ and Simon Schalla, MD, PhD*†‡*

Objectives: Degenerative thoracic aortic aneurysm (TAA) patients are known to be at risk of life-threatening acute aortic events. Guidelines recommend preemptive surgery at diameters of greater than 55 mm, although many patients with small aneurysms show only mild growth rates and more than half of complications occur in aneurysms below this threshold. Thus, assessment of hemodynamics using 4-dimensional flow magnetic resonance has been of interest to obtain more insights in aneurysm development. Nonetheless, the role of aberrant flow patterns in TAA patients is not yet fully understood.

Materials and Methods: A total of 25 TAA patients and 22 controls underwent time-resolved 3-dimensional phase contrast magnetic resonance imaging with 3-directional velocity encoding (ie, 4-dimensional flow magnetic resonance imaging). Hemodynamic parameters such as vorticity, helicity, and wall shear stress (WSS) were calculated from velocity data in 3 anatomical segments of the ascending aorta (root, proximal, and distal). Regional WSS distribution was assessed for the full cardiac cycle.

Results: Flow vorticity and helicity were significantly lower for TAA patients in all segments. The proximal ascending aorta showed a significant increase in peak WSS in the outer curvature in TAA patients, whereas WSS values at the inner curvature were significantly lower as compared with controls. Furthermore, positive WSS gradients from sinotubular junction to midascending aorta were most prominent in the outer curvature, whereas from midascending aorta to brachiocephalic trunk, the outer curvature showed negative WSS gradients in the TAA group. Controls solely showed a positive gradient at the inner curvature for both segments.

Conclusions: Degenerative TAA patients show a decrease in flow vorticity and helicity, which is likely to cause perturbations in physiological flow patterns. The subsequent differing distribution of WSS might be a contributor to vessel wall remodeling and aneurysm formation.

Key Words: magnetic resonance imaging, 4D flow MRI, aorta, aneurysm, aortic aneurysm, hemodynamics

(*Invest Radiol* 2021;56: 494–500)

Thoracic aortic aneurysm (TAA) is defined as a local enlargement of the thoracic aorta to more than 150% of the expected diameter.[1] Despite its asymptomatic character, TAA predisposes for occurrence of life-threatening aortic events (such as dissection or rupture). The risk of natural complications is correlated to the maximal aortic diameter and increases sharply at diameters greater than 60 mm.[2,3] Hence, current clinical guidelines recommend preemptive surgical extirpation of degenerative aneurysms 55 mm or greater (or smaller if concomitant risk factors are present).[4–6] However, more than half of type A dissections occur at diameters below the cutoffs for prophylactic intervention.[7–9] Therefore, there is a need for additional predictors of TAA progression, dissection, and rupture.[10]

Because dissection and rupture are commonly associated with hypertension, there is a developing interest in the role of hemodynamics in the pathophysiology of aortic disease. Four-dimensional flow magnetic resonance imaging (4D flow MRI) is an emerging noninvasive imaging modality that provides comprehensive insight into aortic hemodynamics.[11–13] The technique facilitates acquisition of time-resolved 3-dimensional (3D) 3-directionally encoded velocity data and allows for visualization and quantification of flow patterns and flow-derived hemodynamic markers.[14] To date, abnormal hemodynamics (such as elevated wall shear stress [WSS], flow eccentricity, and flow vorticity) have been linked to different expressions of aortopathy in patients with Marfan syndrome and bicuspid aortic valve (BAV).[15–18] Previous research has described that flow deviations predominantly occur in an aneurysmatic region and that these flow patterns normalize once the aortic diameter normalizes distal from the aneurysmatic area.[19–21] However, flow patterns in patients with degenerative TAA have not quantitatively been characterized, and the potential impact of hemodynamics on development and progression of degenerative aneurysms is not fully understood. The current prospective observational 2-center study aims to characterize regional hemodynamics in the ascending aorta of patients with degenerative TAA and compare findings with those of healthy controls.

MATERIALS AND METHODS

Study Population

Patients with degenerative TAA of 40 mm or greater who visited the outpatient clinic of the Maastricht and Leiden University Medical Centers were prospectively recruited. Exclusion criteria comprised prior aortic or cardiac surgery and the presence of connective tissue disorder, BAV, or general contraindications for MRI. Patients with atrial fibrillation

Received for publication November 10, 2020; and accepted for publication, after revision, January 9, 2021.

From the Departments of *Radiology and Nuclear Medicine, and †Cardiology, Maastricht University Medical Center+; ‡Cardiovascular Research Institute Maastricht, Maastricht University, Maastricht; §Department of Radiology, Leiden University Medical Center; ||Department of Cardiology, Leiden University Medical Center, Leiden; and ¶Department of Chemical Engineering, Transport Phenomena Section, Faculty of Applied Sciences, Delft University of Technology, Delft, the Netherlands.

Conflicts of interest and sources of funding: none declared.

M.J.F.G.R., J.F.J., H.C.v.A., A.J.H.A.S., S.K., H.J.L., J.E.W., J.J.M.W., and S.S. are all funded by the Dutch Heart Foundation (CVON2017-08). B.P.A., J.E.W., S.C.A.M.B., and S.S. are funded by Stichting de Weijerhorst.

Correspondence to: Mitch J.F.G. Ramaekers, MD, Department of Radiology and Nuclear Medicine, Maastricht University Medical Center+, P. Debyelaan 25, 6229 HX, Maastricht, the Netherlands. E-mail: mitch.ramaekers@mumc.nl.

Supplemental digital contents are available for this article. Direct URL citations appear in the printed text and are provided in the HTML and PDF versions of this article on the journal's Web site (www.investigativeradiology.com).

ISSN: 0020-9996/21/5608–0494
DOI: 10.1097/RLI.0000000000000768

TABLE 1. Four-Dimensional Flow MR Acquisition Parameters

	4D Phase Contrast MRI
FOV, mm	350 × 280 × 75
Acquired voxel size, mm	2.5 × 2.5 × 2.5
Reconstructed voxel size, mm	1.46 × 1.46 × 2.5
Flip angle, degrees	10
TE, ms	2.3
TR, ms	4.2
TFE factor	2
SENSE factor	2.5 (P) × 1.5 (S)
VENC, cm/s	150–200
Shot duration, ms	33
(Reconstructed) cardiac phases	24–43

MRI, magnetic resonance imaging; FOV, field of view; TE, echo time; TR, repetition time; TFE, turbo field echo; VENC, velocity encoding.

were excluded to ascertain the accuracy of MR flow measurements. A population of volunteers without aortic or valvular disease was included as control group. The study protocol was approved by the local medical ethical committee, and all subjects provided written informed consent.

Magnetic Resonance Acquisition

Patients underwent MR examinations on 3-T MR systems (Philips Ingenia; Philips Healthcare, Best, the Netherlands). The acquisition protocol included a 4D flow sequence with full volumetric coverage of the left ventricular outflow tract and thoracic aorta. Both medical centers used the same 4D flow sequence (Table 1). Data were acquired using retrospective ECG gating and navigator respiratory gating based on diaphragm excursion. Velocity encoding was typically set at 150 cm/s.

Data Analysis

Image analysis was performed by a single reader (M.R.) using commercially available software (CAAS MR Solutions 5.1; Pie Medical Imaging, Maastricht, the Netherlands). First, the lumen of the aorta was segmented from the magnitude images of the 4D flow data set in peak systole. The segmented mesh was then copied over the entire cardiac cycle for analysis of additional heart phases. Cross-sectional planes were placed at 4 different locations: (1) aortic valve, (2) sinotubular junction (STJ), (3) midascending aorta, and (4) proximal to the origin of brachiocephalic trunk. The cross-sectional planes divided the aorta into 3 segments: aortic root (R), proximal ascending aorta (PAsc), and distal ascending aorta (DAsc) (Fig. 1). The resulting 3 aortic segments were each divided into 4 anatomical regions (anterior and posterior inner curvature and anterior and posterior outer curvature). Wall shear stress was defined as the tangential viscous force acting on the endothelial surface as a result of blood flow and calculated as previously described.[22] Mean WSS values were calculated for each anatomic region

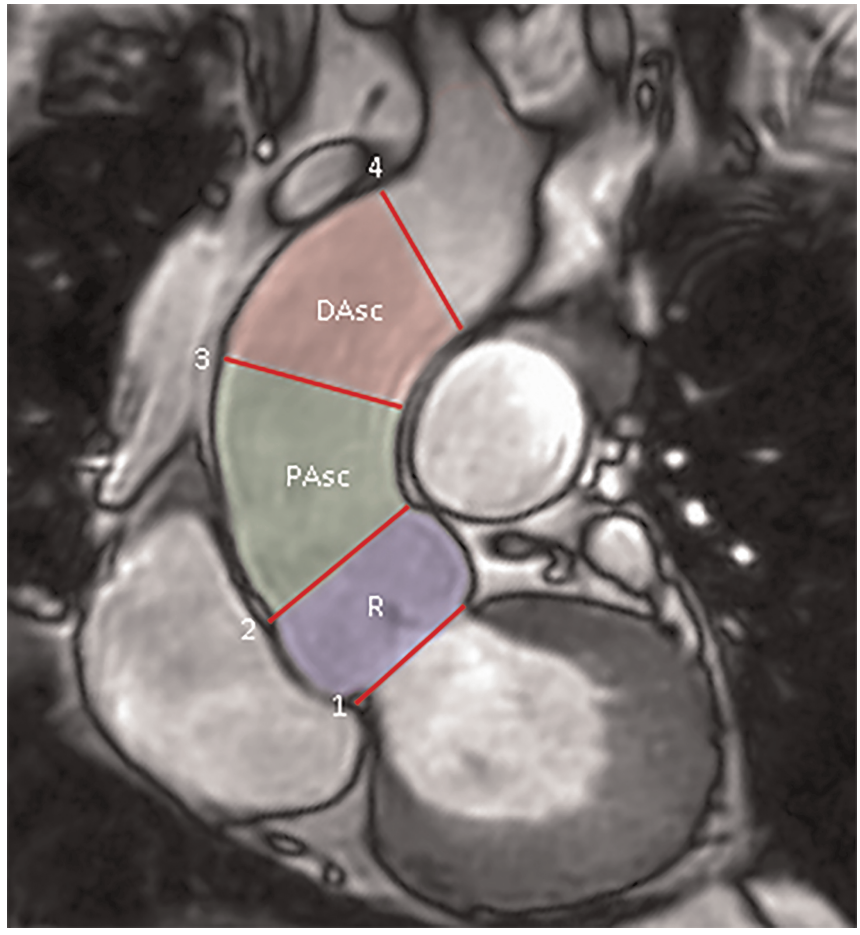

FIGURE 1. Aortic plane placement and division of segments. R indicates aortic root; PAsc, proximal ascending aorta; DAsc, distal ascending aorta.

TABLE 2. Baseline Characteristics of the Study Population

	Controls	TAA	*P*
N	22	25	—
Age, y	63.5 [57.0–67.3]	64.5 [50.8–72.3]	0.790
Men	12 (54.5%)	15 (60.0%)	0.807
BMI, kg/m^2	25.5 [22.5–28.7]	26.4 [23.7–28.7]	0.565
BSA, m^2	1.90 ± 0.26	1.98 ± 0.16	0.281
Hypertension	1 (4.5%)	12 (48%)	0.001*
Hypercholesterolemia	2 (9.1%)	8 (32.0%)	0.079
Diabetes	2 (9.1%)	3 (12.0%)	1.000
Current smoker	4 (18.2%)	4 (16.0%)	1.000
Past smoker	7 (31.8%)	8 (32.0%)	0.989
Medication			
Beta blocker	1 (4.5%)	8 (32.0%)	0.025*
ACE inhibitor	1 (4.5%)	12 (48.0%)	0.001*
Calcium antagonist	0 (0%)	5 (20.0%)	0.052
Nitrate	0 (0%)	0 (0%)	—
Statin	2 (9.1%)	8 (32.0%)	0.079

*Statistically significant.

TAA, thoracic aortic aneurysm; BMI, body mass index; BSA, body surface area; ACE, angiotensin-converting enzyme.

per plane. Flow vorticity ($\vec{\omega}$) was defined as the vector that describes the flow rotation and calculated as follows:

$$\vec{\omega} = \vec{\nabla} \times \vec{v},$$

where $\rightarrow v$ is the velocity vector and $\rightarrow\nabla$ is nabla, the differential operator. Nabla in combination with the cross product (x) is called the rotation operator, or curl. Flow helicity (H) was defined as the dot-product of vorticity with the 3D flow vector and calculated as:

$$H = \vec{v} \cdot \left(\vec{\nabla} \times \vec{v}\right)$$

Flow vorticity magnitude and helicity were both normalized for aortic volume per segment (milliliters) and corrected for stroke volume (milliliters).

Statistical Analysis

Statistical analyses were performed using SPSS Statistics 25 (IBM, Armonk, NY). Normality distribution of the data was tested using the Shapiro-Wilk test. Continuous demographics are expressed as mean ± standard deviation (or as median and interquartile range in the presence of data skewness). Differences between groups were assessed using Student t test (or Mann-Whitney U test, if deemed appropriate). Categorical variables are presented as frequencies and percentages and were evaluated using χ^2 test or Fisher exact test. Correlations between parameters were tested using Spearman R or Pearson correlation coefficient. Gradients were analyzed using a Wilcoxon signed-rank test considering the presence of skewness. A P value of less than 0.05 was considered statistically significant.

RESULTS

A total of 25 TAA patients and 22 controls were included. Patients with TAA were more likely to suffer from hypertension (48.0% vs 4.3%, $P < 0.001$) and to use antihypertensive medication (Table 2). Additional demographics—such as age, sex, and body size—did not differ significantly between groups.

Aortic diameters were significantly larger in TAA patients at all levels of the ascending aorta (plane 2: 41.7 mm vs 34.4 mm, $P < 0.001$; plane 3: 42.7 mm vs 32.5 mm, $P < 0.001$; plane 4: 41.4 mm vs 31.5 mm, $P < 0.001$) (Table 3).

The peak normalized vorticity was significantly lower in the aortic root of TAA patients (64.4 s^{-1} mL^{-2} vs 90.0 s^{-1} mL^{-2}, $P = 0.001$), as well as in the proximal and DAsc (52.6 s^{-1} mL^{-2} vs 74.1 s^{-1} mL^{-2}, $P = 0.013$, and 30.6 s^{-1} mL^{-2} vs 49.5 s^{-1} mL^{-2}, $P = 0.005$, respectively) (Fig. 2A). The peak absolute normalized helicity was significantly lower in TAA patients at the level of the aortic root (5.5 $m{\cdot}s^{-2}{\cdot}mL^{-2}$ vs 7.3 $m{\cdot}s^{-2}{\cdot}mL^{-2}$, $P = 0.001$), PAsc (6.3 $m{\cdot}s^{-2}{\cdot}mL^{-2}$ vs 8.9 $m{\cdot}s^{-2}{\cdot}mL^{-2}$, $P = 0.013$), and DAsc (3.0 $m{\cdot}s^{-2}{\cdot}mL^{-2}$ vs 5.8 $m{\cdot}s^{-2}{\cdot}mL^{-2}$, $P = 0.003$) (Fig. 2B). Besides total values being significantly lower, partial derivatives show distinct differences, whereas areas of high vorticity in controls are mostly located at the inner curvature, whereas TAA patients show a less uniform distribution throughout the lumen (Figs. 3, 4).

Dynamics of WSS over the cardiac cycle for different planes and different regions of the ascending aorta are depicted in Figure 4. In general as compared with controls, peak WSS in TAA patients was lower at the sinuses of Valsalva, whereas it was higher at the outer curvature and lower at the inner curvature at the PAsc and returning to lower values at the DAsc. The peak WSS was significantly lower at the level of the sinuses of Valsalva in TAA patients at the posterior part of the inner curvature (729 mPa vs 955 mPa, $P = 0.026$), the anterior part of the inner curvature (652 mPa vs 874 mPa, $P = 0.036$), and the posterior part of the outer curvature (769 mPa vs 979 mPa, $P = 0.049$). The peak WSS was significantly lower at the anterior part of the inner curvature of the PAsc in TAA patients (734 mPa vs 864 mPa, $P = 0.026$), whereas it turned out to be significantly higher at the anterior part of the outer curvature (1285 mPa vs 963 mPa, $P = 0.007$). The DAsc showed significantly lower peak WSS values in TAA patients at the anterior area of the inner curvature (773 mPa vs 986 mPa, $P = 0.006$), the posterior area of the inner curvature (936 mPa vs 1306 mPa, $P < 0.001$), and the posterior area of the outer curvature (707 mPa vs 947 mPa, $P = 0.001$). The peak WSS did not differ significantly at other regions.

Of note, the positive peak WSS gradients were observed between the STJ and PAsc in TAA patients at the outer curvature posterior (769–1119 mPa, $P = 0.007$), at the outer curvature anterior (839–1285 mPa, $P < 0.001$), and at the inner curvature posterior (729–938 mPa, $P = 0.004$), whereas controls only showed a significant positive gradient at the inner curvature posterior from STJ to PAsc (955–1138 mPa, $P = 0.027$). From PAsc to DAsc, a negative gradient is seen in TAA patients at the outer curvature posterior and anterior (1119–707 mPa, $P < 0.001$ and 1285–964 mPa, $P = 0.002$, respectively). Controls showed a positive gradient between PAsc and DAsc

TABLE 3. Ascending Aortic Dimensions

	Controls (n = 22)	TAA (n = 25)	*P*
Maximal diameter root, mm	34.3 ± 4.5	41.7 ± 6.0	<0.001*
Maximal diameter PAsc, mm	32.5 ± 4.1	42.7 ± 4.5	<0.001*
Maximal diameter DAsc, mm	31.5 ± 4.2	41.4 ± 4.2	<0.001*
Centerline length root, mm	15.7 ± 3.4	17.2 ± 3.6	0.151
Centerline length PAsc, mm	28.5 ± 4.7	33.3 ± 9.3	0.031*
Centerline length DAsc, mm	30.3 ± 5.2	41.0 ± 9.73	<0.001*

Maximal aortic diameters (in millimeter) of the study population are measured at 3 levels of the ascending aorta. Centerline length (in millimeter) is measured in all 3 segments of the ascending aorta.

*Statistically significant.

TAA, thoracic aortic aneurysm; PAsc, proximal ascending aorta; DAsc, distal ascending aorta.

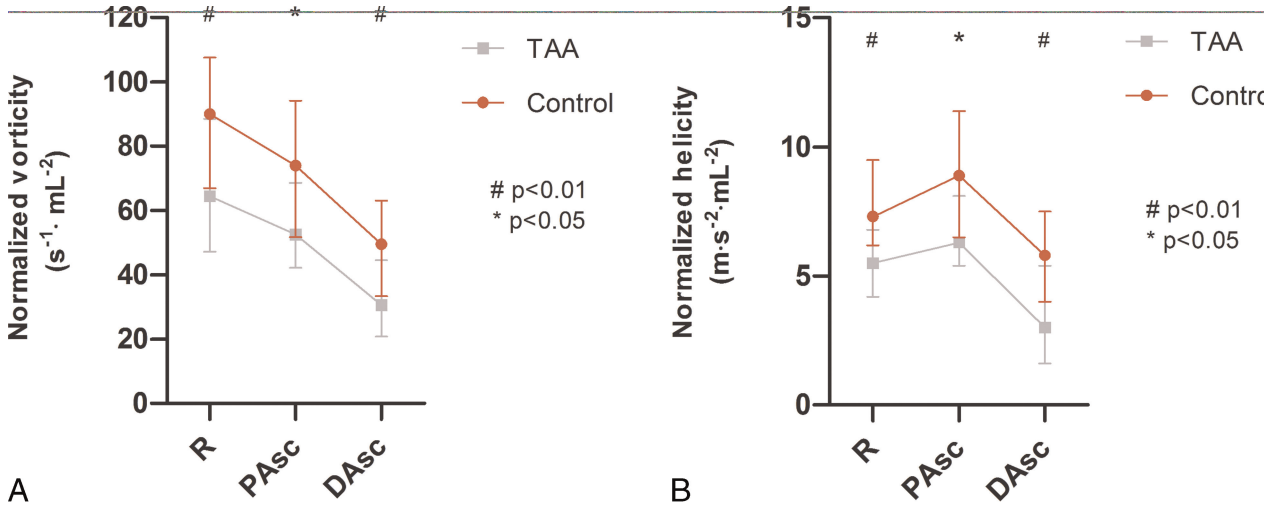

FIGURE 2. A, Flow vorticity normalized for aortic volume and stroke volume (s^{-1} mL^{-2}). A, Image shows the flow vorticity through the ascending aorta in controls (red) and thoracic aortic aneurysm (TAA) patients (gray). *$P < 0.05$; #$P < 0.01$. B, Absolute flow helicity normalized for aortic volume and stroke volume ($m{\cdot}s^{-2}{\cdot}mL^{-2}$). B, Image depicts the flow helicity through the ascending aorta in controls (red) and TAA patients (gray). R indicates aortic root; PAsc, proximal ascending aorta; DAsc, distal ascending aorta. *$P < 0.05$; #$P < 0.01$.

for the inner curvature posterior and anterior (1138–1306 mPa, $P = 0.003$ and 864–992 mPa, $P = 0.008$, respectively) (Figs. 5, 6).

DISCUSSION

In the current study, we assessed hemodynamic parameters in the ascending aortas of patients with degenerative TAA and compared them to those in healthy controls. We found that TAA patients (1) have decreased normalized aortic flow vorticity and helicity, (2) show more asymmetrically distributed peak WSS values with elevated WSS at the outer curvature and decreased WSS at the inner curvature, and (3) show a positive WSS gradient from the sinotubular junction to the PAsc.

Aberrant Flow Patterns

Physiological vorticity and helicity play a role in maintaining stable flow through the aorta.[19,23] According to Poiseuille's law of flow in a U-bend shape, such as the thoracic aorta, centripetal forces in the proximal part cause a shift of the parabolic peak velocity from the center of aorta to the inner curvature, where distally in the U-bend, centrifugal forces dominate and cause a shift toward the outer curvature. The secondary flow patterns that occur as a consequence, consisting of 2 counter rotating in-plane vortices, are needed to maintain stable flow and mass transportation. In the current study, these secondary flow patterns were clearly seen in controls when taking a look at the rotation components of the flow vorticity, whereas the pattern in TAA patients was found to be different (Figs. 3, 4). These secondary flow patterns in the healthy aorta have been demonstrated to compensate for the adverse effects of the aortic curvature on blood flow, hence sparing the ascending aorta and arch from low-density lipoprotein deposition and atherogenesis.[24] The normal aortic aging process involves luminal dilatation and elongation, which occur in association with decreased flow helicity and vorticity.[23,25,26] Changes in blood flow have been of increasing interest in patients with aortic disease. Recent 4D flow MR studies reported pronounced helical and vortical flow patterns in patients with TAA, connective tissue disease, and BAV.[17,19,27] However, most of these studies used qualitative observations using stream- or path-line analysis, which are prone for bias and difficult to analyze regarding the secondary in-plane flow patterns. Only 1 previous study quantified flow vorticity in the ascending aorta in patients with BAV, showing increased vorticity as compared with healthy controls.[28] Yet, given that a substantial part of the included BAV population had

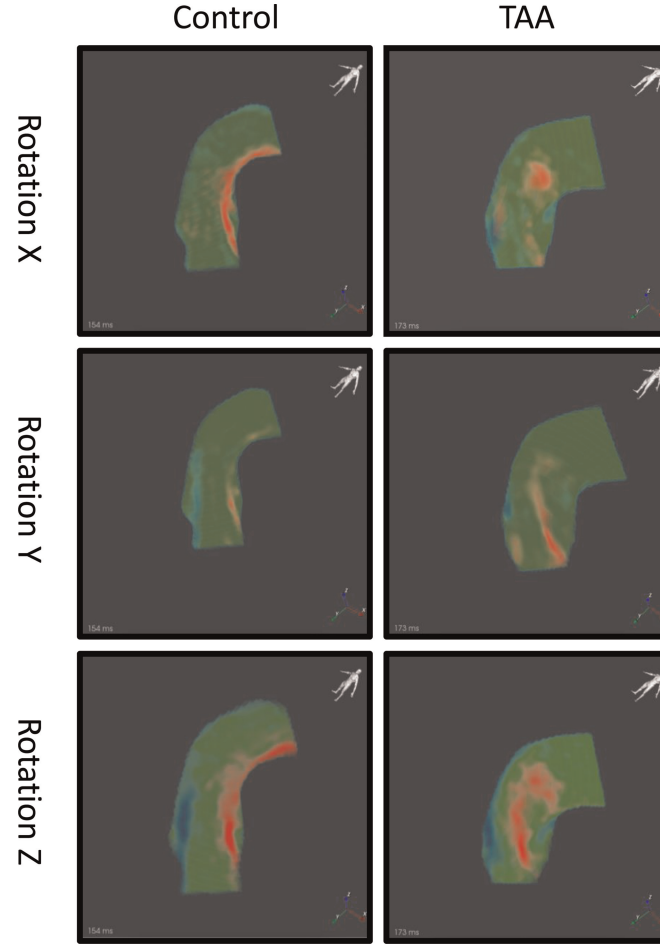

FIGURE 3. Separate components of rotation in vorticity calculation. Images depict values of a central vertical plane of a single representative subject per group. Red and blue are positive and negative values, respectively.

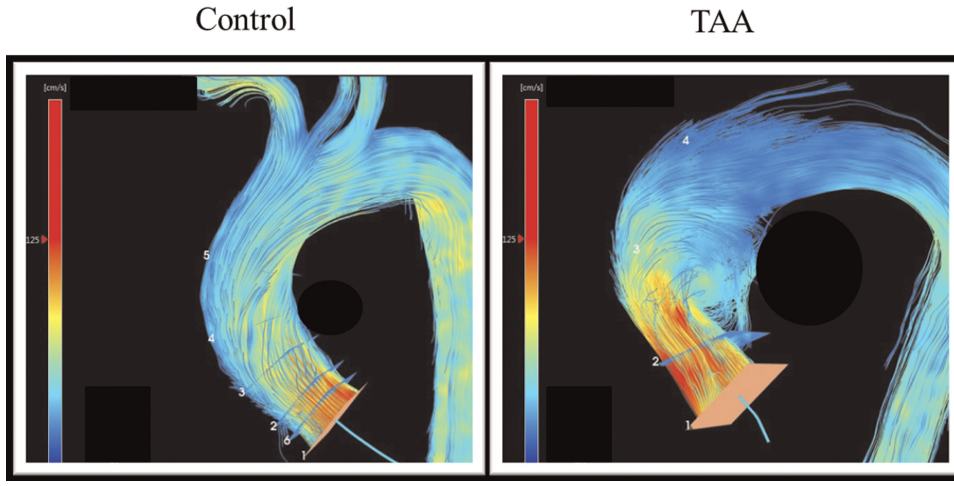

FIGURE 4. Visualization of ascending aortic flow velocities and flow directions in the systolic heart phase with most pronounced flow perturbations of a TAA patient and a healthy control. Blue and red indicate low and high velocity, respectively. Full videos of flow patterns in these subjects are available as Supplemental Digital Content (see videos Supplemental Digital Content 1 and 2, showing ascending aortic flow patterns, http://links.lww.com/RLI/A610, http://links.lww.com/RLI/A611).

dysfunctional valves with concomitant high peak flow velocities, this result could be foreseen when looking at the formula to calculate vorticity. Compared with healthy controls and as opposed to BAV, we found a decrease in flow vorticity and helicity in degenerative ascending aortic aneurysms. We hypothesize that the transformations of aortic dimensions with increasing age lead to substantial perturbations in the in-plane vorticity, with abnormal flow patterns as a consequence. Moreover, subsequently to the need of vorticity and helicity to stabilize flow, declining vorticity and helicity increases the risk of flow abnormalities such as flow separation. Flow separation might occur with diminishing secondary in-plane vortices and are a possible cause of large "slow" vortices in TAA patients. It is proposed that this could lead to unequal distribution of WSS, with more risk of low-density lipoprotein transportation along the side of the vessel wall that experiences low WSS.[24]

Wall Shear Stress

Wall shear stress is an important parameter when describing the mechanotransduction of flow stresses on the vessel wall. Both low and high WSS play a role in the pathophysiology of aortic disease. Results from in vitro studies indicate that elevated WSS contributes to aortic dilatation, whereas low WSS is associated with atherosclerotic plaque formation.[29,30] High WSS and positive WSS gradients have been shown to result in adapted gene expression in endothelial cells, which initiates endothelial proliferation, extracellular matrix degradation, and aneurysm

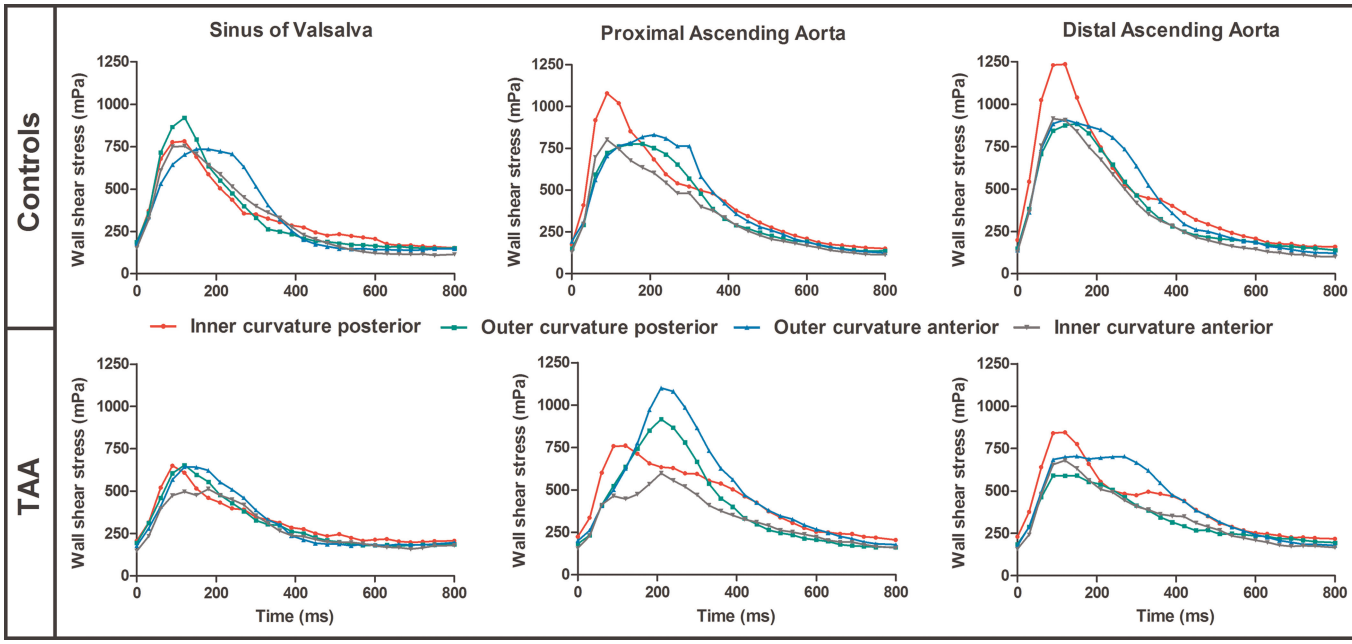

FIGURE 5. Wall shear stress dynamics over the cardiac cycle. The graphs depict the wall shear stress for both groups in 3 planes, subdivided in 4 regions: inner curvature posterior (ICA, red), outer curvature posterior (OCP, green), outer curvature anterior (OCA, blue), and inner curvature anterior (ICA, dark gray).

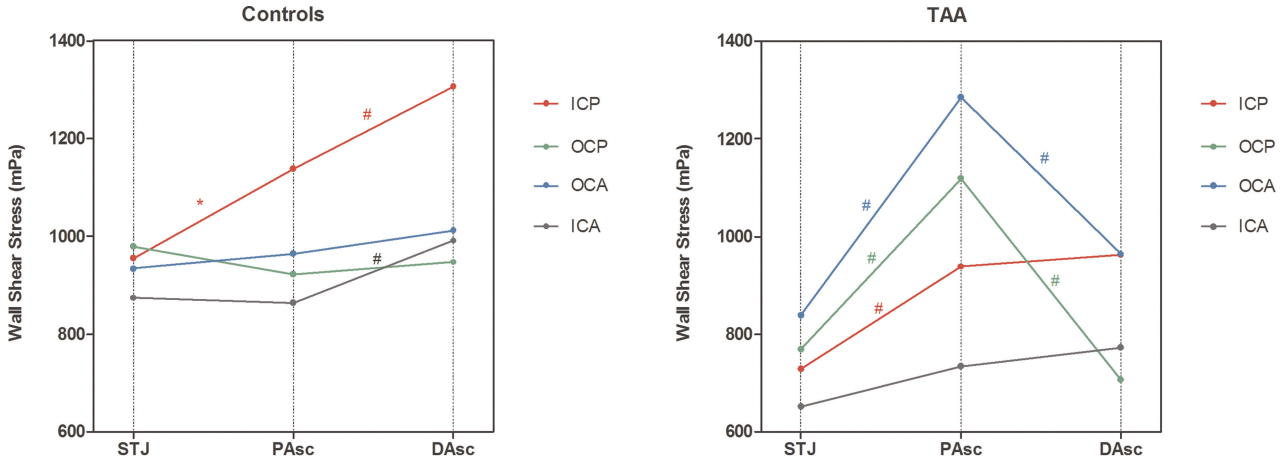

FIGURE 6. Gradients of wall shear stress from proximal to distal in the ascending aorta. STJ, sinotubular junction; PAsc, proximal ascending aorta; DAsc, distal ascending aorta; ICP, inner curvature posterior; OCP, outer curvature posterior; OCA, outer curvature anterior; ICA, inner curvature anterior.

formation.[30] Mahadevia et al[17] used 4D flow MRI and found a relationship between different BAV fusion patterns and the location of peak ascending aortic WSS, which might be part of the link between BAV and the associated aortopathy. Moreover, a high ratio of circumferential to total WSS has been described as a cause of poststenotic aortic dilatation (ie, aneurysm formation distal to a stenotic aortic valve).[31]

Contrary to studies that have observed an association between elevated WSS and vessel dilatation, there is evidence that rupture of aneurysms occurs at regions of low WSS. It is hypothesized that low WSS and thrombus deposition predominates at regions of flow recirculation, which results in adventitial degeneration and subsequent aneurysm rupture.[32] One previous 4D flow MR study concluded that TAA patients exhibit significantly lower WSS in all aortic segments and regions during peak systole.[19] Our results do not support this conclusion. First, we found that WSS is asymmetrically distributed around the vessel wall. Although the averaged WSS per segment may be lower in TAA, we have demonstrated that peak WSS in the outer aortic curvature was significantly higher as compared with controls. Second, due to aberrant flow patterns, awareness for looking beyond peak systole rises, because these flow patterns occur more toward the end systole.[33] A discrepancy between peak systole and peak WSS might be a plausible cause for deviating results as compared with the earlier study.[19] Along with the positive WSS gradient, this elevated peak WSS could promote aortic dilation in this region.

Mechano-sensing of WSS and other mechanical stresses in the arterial wall are of great importance.[34] The exact influence of aberrant flow and deviated WSS on mechanotransduction deserves further evaluation, considering a previously described association of aortic stiffness with aortic disease progression[35]: an interesting goal for future studies would thus be to evaluate MR methods that combine flow analysis and markers of vessel wall stiffness such as pulse wave velocity and MR elastography.[36–38]

Study Limitations

Some limitations of the current study need to be addressed. First, the accuracy of WSS estimations by 4D flow MR is limited by the technique's inherent spatial and temporal resolution. Consequently, WSS estimations are consistently lower than those derived from model-based computational fluid dynamics simulations (which have arbitrary high spatial and temporal resolution).[39] However, the MR acquisition protocol was similar for all study subjects, which allows for reliable WSS comparison between patient groups.

Second, we created a static 3D geometry during peak systole and used this to calculate WSS, vorticity, and helicity over the cardiac cycle. This approach neglects potential cyclic movement and distensibility of the ascending aorta. However, segmentation was performed on velocity data, making it infeasible to create accurate geometric models in phases with low flow velocities (especially diastole).

We found a decrease of flow vorticity and helicity and an unequal distribution of WSS with higher peak WSS in TAA patients. The decrease of helicity and vorticity are a possible cause of aberrant flow in degenerative TAAs, which is likely to induce the unequal distribution of WSS. These variations in peak WSS and WSS gradients are potential contributors to vessel wall remodeling and thus could promote further aortic dilation.

REFERENCES

1. Goldstein SA, Evangelista A, Abbara S, et al. Multimodality imaging of diseases of the thoracic aorta in adults: from the American Society of Echocardiography and the European Association of Cardiovascular Imaging: endorsed by the Society of Cardiovascular Computed Tomography and Society for Cardiovascular Magnetic Resonance. *J Am Soc Echocardiogr*. 2015;28:119–182.
2. Davies RR, Goldstein LJ, Coady MA, et al. Yearly rupture or dissection rates for thoracic aortic aneurysms: simple prediction based on size. *Ann Thorac Surg*. 2002;73:17–27.
3. Coady MA, Rizzo JA, Hammond GL, et al. What is the appropriate size criterion for resection of thoracic aortic aneurysms? *J Thorac Cardiovasc Surg*. 1997;113:476–491; discussion 89–91.
4. Coady MA, Rizzo JA, Hammond GL, et al. Surgical intervention criteria for thoracic aortic aneurysms: a study of growth rates and complications. *Ann Thorac Surg*. 1999;67:1922–1926; discussion 53–58.
5. Erbel R, Aboyans V, Boileau C, et al. 2014 ESC guidelines on the diagnosis and treatment of aortic diseases: document covering acute and chronic aortic diseases of the thoracic and abdominal aorta of the adult. The Task Force for the Diagnosis and Treatment of Aortic Diseases of the European Society of Cardiology (ESC). *Eur Heart J*. 2014;35:2873–2926.
6. Hiratzka LF, Bakris GL, Beckman JA, et al. 2010 ACCF/AHA/AATS/ACR/ASA/SCA/SCAI/SIR/STS/SVM Guidelines for the diagnosis and management of patients with thoracic aortic disease. A Report of the American College of Cardiology Foundation/American Heart Association Task Force on Practice Guidelines, American Association for Thoracic Surgery, American College of Radiology, American Stroke Association, Society of Cardiovascular Anesthesiologists, Society for Cardiovascular Angiography and Interventions, Society of Interventional Radiology, Society of Thoracic Surgeons, and Society for Vascular Medicine. *J Am Coll Cardiol*. 2010;55:e27–e129.
7. Pape LA, Tsai TT, Isselbacher EM, et al. Aortic diameter >or = 5.5 cm is not a good predictor of type A aortic dissection: observations from the international registry of acute aortic dissection (IRAD). *Circulation*. 2007;116:1120–1127.
8. Heuts S, Adriaans BP, Gerretsen S, et al. Aortic elongation part II: the risk of acute type A aortic dissection. *Heart*. 2018;104:1778–1782.
9. Heuts S, Adriaans BP, Rylski B, et al. Evaluating the diagnostic accuracy of maximal aortic diameter, length and volume for prediction of aortic dissection. *Heart*. 2020;106:892–897.

10. Adriaans BP, Wildberger JE, Westenberg JJM, et al. Predictive imaging for thoracic aortic dissection and rupture: moving beyond diameters. *Eur Radiol*. 2019; 29:6396–6404.
11. Dyverfeldt P, Bissell M, Barker AJ, et al. 4D flow cardiovascular magnetic resonance consensus statement. *J Cardiovasc Magn Reson*. 2015;17:72.
12. Frydrychowicz A, Markl M, Hirtler D, et al. Aortic hemodynamics in patients with and without repair of aortic coarctation: in vivo analysis by 4D flow-sensitive magnetic resonance imaging. *Invest Radiol*. 2011;46:317–325.
13. Catapano F, Pambianchi G, Cundari G, et al. 4D flow imaging of the thoracic aorta: is there an added clinical value? *Cardiovasc Diagn Ther*. 2020;10:1068–1089.
14. Markl M, Frydrychowicz A, Kozerke S, et al. 4D flow MRI. *J Magn Reson Imaging*. 2012;36:1015–1036.
15. Geiger J, Hirtler D, Gottfried K, et al. Longitudinal evaluation of aortic hemodynamics in Marfan syndrome: new insights from a 4D flow cardiovascular magnetic resonance multi-year follow-up study. *J Cardiovasc Magn Reson*. 2017;19:33.
16. Barker AJ, Markl M, Bürk J, et al. Bicuspid aortic valve is associated with altered wall shear stress in the ascending aorta. *Circ Cardiovasc Imaging*. 2012;5:457–466.
17. Mahadevia R, Barker AJ, Schnell S, et al. Bicuspid aortic cusp fusion morphology alters aortic three-dimensional outflow patterns, wall shear stress, and expression of aortopathy. *Circulation*. 2014;129:673–682.
18. Bissell MM, Hess AT, Biasiolli L, et al. Aortic dilation in bicuspid aortic valve disease: flow pattern is a major contributor and differs with valve fusion type. *Circ Cardiovasc Imaging*. 2013;6:499–507.
19. Burk J, Blanke P, Stankovic Z, et al. Evaluation of 3D blood flow patterns and wall shear stress in the normal and dilated thoracic aorta using flow-sensitive 4D CMR. *J Cardiovasc Magn Reson*. 2012;14:84.
20. Hope TA, Markl M, Wigström L, et al. Comparison of flow patterns in ascending aortic aneurysms and volunteers using four-dimensional magnetic resonance velocity mapping. *J Magn Reson Imaging*. 2007;26:1471–1479.
21. Kilner PJ, Yang GZ, Mohiaddin RH, et al. Helical and retrograde secondary flow patterns in the aortic arch studied by three-directional magnetic resonance velocity mapping. *Circulation*. 1993;88:2235–2247.
22. Stalder AF, Russe MF, Frydrychowicz A, et al. Quantitative 2D and 3D phase contrast MRI: optimized analysis of blood flow and vessel wall parameters. *Magn Reson Med*. 2008;60:1218–1231.
23. Callaghan FM, Bannon P, Barin E, et al. Age-related changes of shape and flow dynamics in healthy adult aortas: a 4D flow MRI study. *J Magn Reson Imaging*. 2019;49:90–100.
24. Liu X, Pu F, Fan Y, et al. A numerical study on the flow of blood and the transport of LDL in the human aorta: the physiological significance of the helical flow in the aortic arch. *Am J Physiol Heart Circ Physiol*. 2009;297:H163–H170.
25. Adriaans BP, Heuts S, Gerretsen S, et al. Aortic elongation part I: the normal aortic ageing process. *Heart*. 2018;104:1772–1777.
26. Wolak A, Gransar H, Thomson LE, et al. Aortic size assessment by noncontrast cardiac computed tomography: normal limits by age, gender, and body surface area. *JACC Cardiovasc Imaging*. 2008;1:200–209.
27. van der Palen RL, Barker AJ, Bollache E, et al. Altered aortic 3D hemodynamics and geometry in pediatric Marfan syndrome patients. *J Cardiovasc Magn Reson*. 2017;19:30.
28. Elbaz MSM, Scott MB, Barker AJ, et al. Four-dimensional virtual catheter: noninvasive assessment of intra-aortic hemodynamics in bicuspid aortic valve disease. *Radiology*. 2019;293:541–550.
29. Cheng C, Tempel D, van Haperen R, et al. Atherosclerotic lesion size and vulnerability are determined by patterns of fluid shear stress. *Circulation*. 2006;113: 2744–2753.
30. Dolan JM, Kolega J, Meng H. High wall shear stress and spatial gradients in vascular pathology: a review. *Ann Biomed Eng*. 2013;41:1411–1427.
31. Kauhanen SP, Hedman M, Kariniemi E, et al. Aortic dilatation associates with flow displacement and increased circumferential wall shear stress in patients without aortic stenosis: a prospective clinical study. *J Magn Reson Imaging*. 2019;50:136–145.
32. Boyd AJ, Kuhn DC, Lozowy RJ, et al. Low wall shear stress predominates at sites of abdominal aortic aneurysm rupture. *J Vasc Surg*. 2016;63:1613–1619.
33. von Spiczak J, Crelier G, Giese D, et al. Quantitative analysis of vortical blood flow in the thoracic aorta using 4D phase contrast MRI. *PLoS One*. 2015;10:e0139025.
34. Humphrey JD, Schwartz MA, Tellides G, et al. Role of mechanotransduction in vascular biology: focus on thoracic aortic aneurysms and dissections. *Circ Res*. 2015;116:1448–1461.
35. Boczar KE, Boodhwani M, Beauchesne L, et al. Aortic stiffness, central blood pressure, and pulsatile arterial load predict future thoracic aortic aneurysm expansion. *Hypertension*. 2021;77:126–134.
36. Shahzad R, Shankar A, Amier R, et al. Quantification of aortic pulse wave velocity from a population based cohort: a fully automatic method. *J Cardiovasc Magn Reson*. 2019;21:27.
37. Dong H, Russell DS, Litsky AS, et al. In vivo aortic magnetic resonance elastography in abdominal aortic aneurysm: a validation in an animal model. *Invest Radiol*. 2020;55:463–472.
38. Schaafs LA, Tzschätzsch H, Reshetnik A, et al. Ultrasound time-harmonic elastography of the aorta: effect of age and hypertension on aortic stiffness. *Invest Radiol*. 2019;54:675–680.
39. Szajer J, Ho-Shon K. A comparison of 4D flow MRI-derived wall shear stress with computational fluid dynamics methods for intracranial aneurysms and carotid bifurcations—a review. *Magn Reson Imaging*. 2018;48:62–69.